Forschungszentrum Karlsruhe
in der Helmholtz-Gemeinschaft

Wissenschaftliche Berichte
FZKA 6764

A nuclear simulation experiment for the International Fusion Materials Irradiation Facility (IFMIF)

U. von Möllendorff, F. Maekawa*, H. Giese, H. Feuerstein
Institut für Reaktorsicherheit
Institut für Hochleistungsimpuls- und Mikrowellentechnik
Hauptabteilung Ingenieurtechnik
Programm Kernfusion

*Japan Atomic Energy Research Institute

Forschungszentrum Karlsruhe GmbH, Karlsruhe
2002

Impressum der Print-Ausgabe:

Als Manuskript gedruckt

Forschungszentrum Karlsruhe GmbH
Postfach 3640, 76021 Karlsruhe

Mitglied der Hermann von Helmholtz-Gemeinschaft
Deutscher Forschungszentren (HGF)

ISSN 0947-8620

Abstract
For studying neutronic and nuclear characteristics of the projected International Fusion Materials Irradiation Facility (IFMIF), a saturation thick target of natural lithium was irradiated with 40 MeV deuterons from the Karlsruhe Isochronous Cyclotron. The resulting neutron spectrum and yield were measured by multi-foil activation. The production rates of the radionuclides tritium and beryllium-7 in the lithium were also measured. They are (6.85 g ± 7%) tritium and (1.85 g ± 12%) Be-7 per IFMIF full power year at 40 MeV and 250 mA; these values supersede preliminary results given earlier. Further, samples of two different steels, pure vanadium, and a vanadium alloy were activated in the neutron field, and specific activities of many radionuclides in becquerel per kg of material subsequently determined by gamma spectrometry. The report gives all experimental results together with sufficient experimental details to enable calculations for testing nuclear data.

Ein nukleares Simulationsexperiment für die International Fusion Materials Irradiation Facility (IFMIF)

Zusammenfassung
Zur Untersuchung von neutronischen und nuklearen Charakteristika der projektierten International Fusion Materials Irradiation Facility (IFMIF) wurde ein sättigungsdickes natürliches Lithiumtarget mit 40-MeV-Deuteronen aus dem Karlsruher Isochronzyklotron bestrahlt. Spektrum und Ausbeute der entstehenden Neutronen wurden mittels Multifolien-Aktivierung gemessen. Auch die Erzeugungsraten der Radionuklide Tritium und Beryllium-7 im Lithium wurden gemessen. Sie betragen (6.85 g ± 7%) Tritium and (1.85 g ± 12%) Be-7 pro IFMIF-Volleistungsjahr bei 40 MeV and 250 mA; diese Werte ersetzen früher angegebene vorläufige Ergebnisse. Außerdem wurden Proben von zwei verschiedenen Stählen, reinem Vanadium und einer Vanadiumlegierung in dem Neutronenfeld aktiviert und anschließend durch Gammaspektrometrie spezifische Aktivitäten vieler Radionuklide in Becquerel pro kg Material bestimmt. Der Bericht enthält alle Meßergebnisse zusammen mit genügend experimentellen Einzelheiten, um Vergleichsberechnungen zur Prüfung von Kerndaten zu ermöglichen.

Contents Page

1 INTRODUCTION

Within the Conceptual Design Evaluation (CDE) phase (1997-1998) of the International Fusion Materials Irradiation Facility (IFMIF) project, an experiment simulating the nuclear features of the IFMIF neutron source was performed. The analysis of the experimental results extended into the subsequent Key Element technology Phase (KEP) of the project.

At the Karlsruhe Isochronous Cyclotron a beam of about 3 μA of 40-MeV deuterons impinged on a saturation thick target of natural lithium. This deuteron current is almost 5 orders of magnitude less than the envisaged current in IFMIF, 250 mA. It nevertheless provides a valid simulation of the IFMIF neutron source, because, even at 250 mA, the interaction of a deuteron or a neutron with a nucleus occurs independently of any similar interaction events in the vicinity. Therefore, the interaction rates are precisely proportional to the particle flux, and quantities such as the neutron yield per deuteron, the shape of the neutron spectrum, etc, are independent of the current.

Several quantities were measured in this experiment. The results represent additional contributions to the Tasks defined for the KEP as follows:

Measured quantity	*KEP Task*
Neutron spectrum and flux	TF51-EU
Tritium and beryllium-7 production rates in the lithium	TF51-EU (TF34-JA)
Production rates of various radionuclides in samples of four different structural materials exposed to the neutron field	TF54-EU

Results for the neutron spectrum (but not in numerical form) were already reported in Ref.[Ma00]. Very preliminary results for the H-3 and Be-7 production were reported in Ref.[Mö99]. The results for neutron-induced radioactivity in structural materials were given in the form of calculation-over-experiment *(C/E)* ratios in Ref.[Mö00], based on calculations made with IEAF-99, an early version of the Intermediate Energy Activation File [Ko01]. However, the experimental activation results proper, i.e., the specific activities in Bq per kg of sample material obtained at different cooling times, have not been documented so far. These, as well as the neutron spectrum in numerical form and sufficient details of the irradiations are given here, so that the results of this experiment can be used for comparison with calculations using any present or future codes and cross section libraries.

2 TARGETS AND IRRADIATIONS

2.1 General remarks

Metallic lithium is chemically reactive, especially in a normal atmosphere containing moisture, and is evaporated easily. Moreover, for reasons of beam availability it was necessary to use an internal target, i.e., a target positioned within the cyclotron itself rather than in an external beam line. For safety and convenience in handling, therefore, it was decided to use a target enclosed in a steel container.

This had the additional advantage that the upstream steel wall, which the deuteron beam had to pass through before interacting with the lithium, acted as a beam energy degrader, so that the full deuteron energy of the available (fixed-energy) cyclotron, 52 MeV, could be utilized. With proper choice of thickness, 1.1 mm, the steel wall takes away 12 MeV from incident 52-MeV deuterons[Zi85]. Thus, the deuterons entered the lithium layer with an energy of 40 MeV, as specified for IFMIF. Any deuteron beam energy lower than 52 MeV would have been available at this cyclotron only by positioning the target some way inside the cyclotron magnet gap, so that it cuts into the spiralling beam trajectory, which means that the beam will hit the target only near one of its edges. With the full energy, however, the 'lifted' beam could be used, i.e., the beam was deflected away from its preceding turn by several millimeters using an electrostatic septum, as if it were to be extracted to a beam line. This permitted us to position the beam spot close to the centre of the 24 mm by 34 mm target front face.

Since one of the goals was the subsequent determination of accumulated tritium, it was important to select a container material having not only high corrosion resistance to lithium but also negligible tritium permeation at the expected temperatures during irradiation (up to about 400°C). Among known and available materials, the standard austenitic stainless steel DIN 1.4571, very similar to the well known SS-316, is favourable in this respect and was selected.

A disadvantage of this choice is the low thermal conductivity of the steel, which limited the possibility to cool the target in view of the beam power of 52 W per microampere deposited in it.

Deuteron interaction with the upstream container wall inevitably produces some neutrons in addition to those generated in the lithium. Therefore, a separate measurement of this neutron background was made, using a specially designed empty target consisting of the same type of steel.

2.2 Lithium target

Fig. 2-1 shows a drawing of the lithium target. The target consists of an upper part (hood) of steel, with a space to hold the lithium, and a lower part (foot) of aluminium, through which cooling water is supplied. In modelling the target for calculations of neutron production, the big iron pole pieces of the cyclotron magnet should be included; Fig.2-2, therefore, shows the target in its irradiation position near the rims of these two circular, mirror symmetric parts. Both of the drawings are slightly simplified, but sufficiently accurate for characterizing the target and its environment with respect to neutron interactions.

The target hood was machined from a block of 1.4571 steel. After filling it with pure natural lithium in a glove box, a close fitting lid of the same steel was put on and the target was closed by laser beam welding. Filling, transportation and welding were all done in an argon atmosphere.

Three nominally identical target hoods were produced in this way, with lithium content varying from 4.23 to 4.42 g. This corresponds to about 85% of the available volume. The remaining argon-filled space in the container is useful to take up the pressure rise due to thermal expansion under irradiation. The position of the target during irradiation is the same as seen in the lower part of Fig. 2-1, i.e. the short sides of the box-shaped container facing up and down, with the cyclotron magnet pole plates horizontally above and below. Assuming that the lithium is melted by the beam heat (melting temperature 185°C), the argon bubble will be at the top of the volume and thus outside the region reached by the deuterons.

For the neutron spectrum measurement, two packs of activation foils were used simultaneously in the two positions provided by the sample holder (labeled ‘Detail A’ in Fig. 2-1). One position covered in a symmetrical way an emission angular range around 0° (‘Centre’). The other was shifted by 7.0 mm downward, at right angles to the beam direction (‘Side’), so as to get at least some rough information about the angular distribution of the source neutrons. All samples and activation foils were of square shape, 5 mm by 5 mm in size.

2.3 Empty target

The background neutron measurement with a target hood not containing lithium is complicated by the fact that the empty container will not stop the deuteron beam. Therefore, its downstream wall must have an opening for the outgoing beam to avoid additional neutron production there, and dosimetry foils may be placed only to the side of that (somewhat diver-

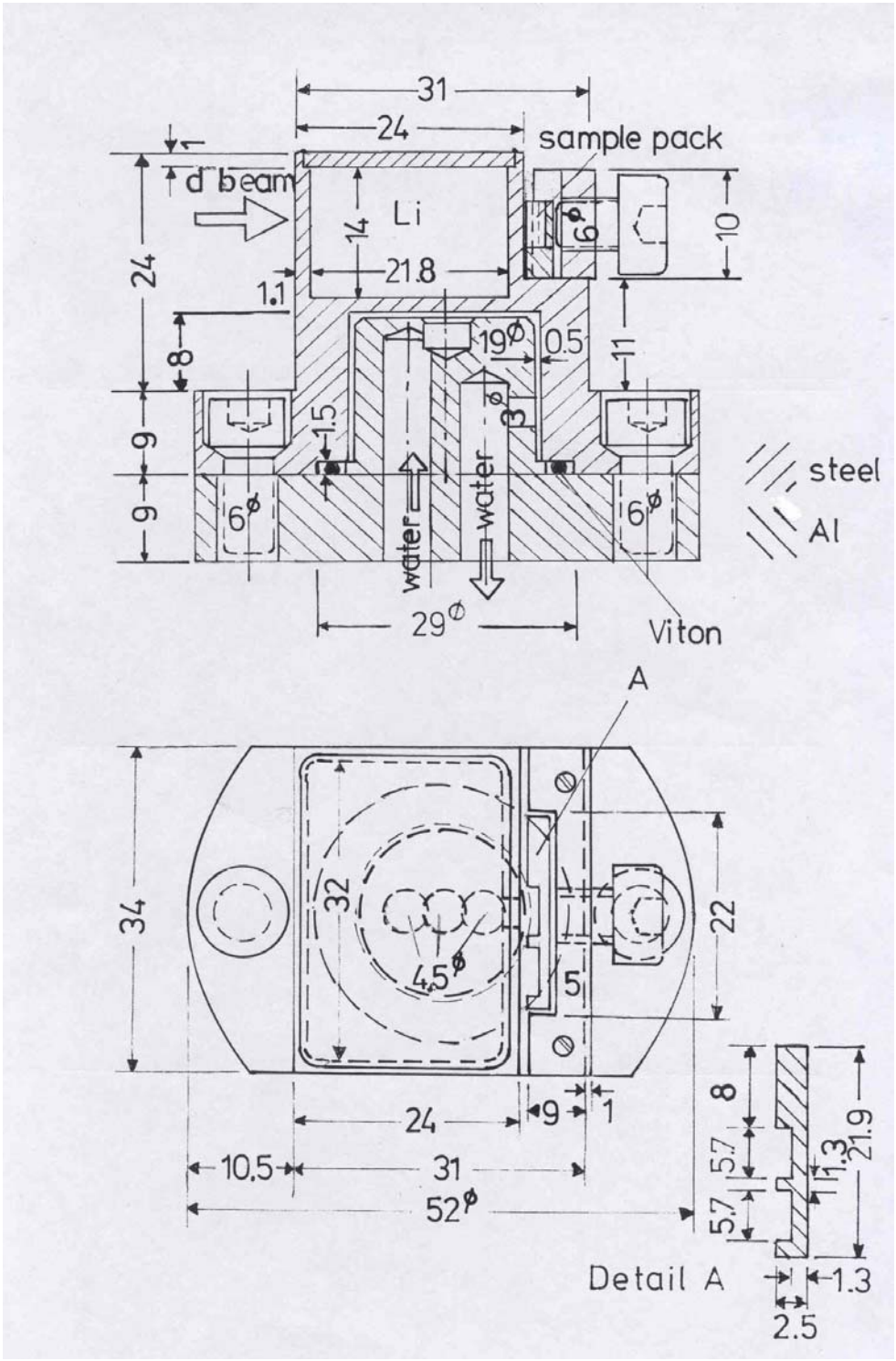

Figure 2-1 Lithium-filled target

All screws are stainless steel

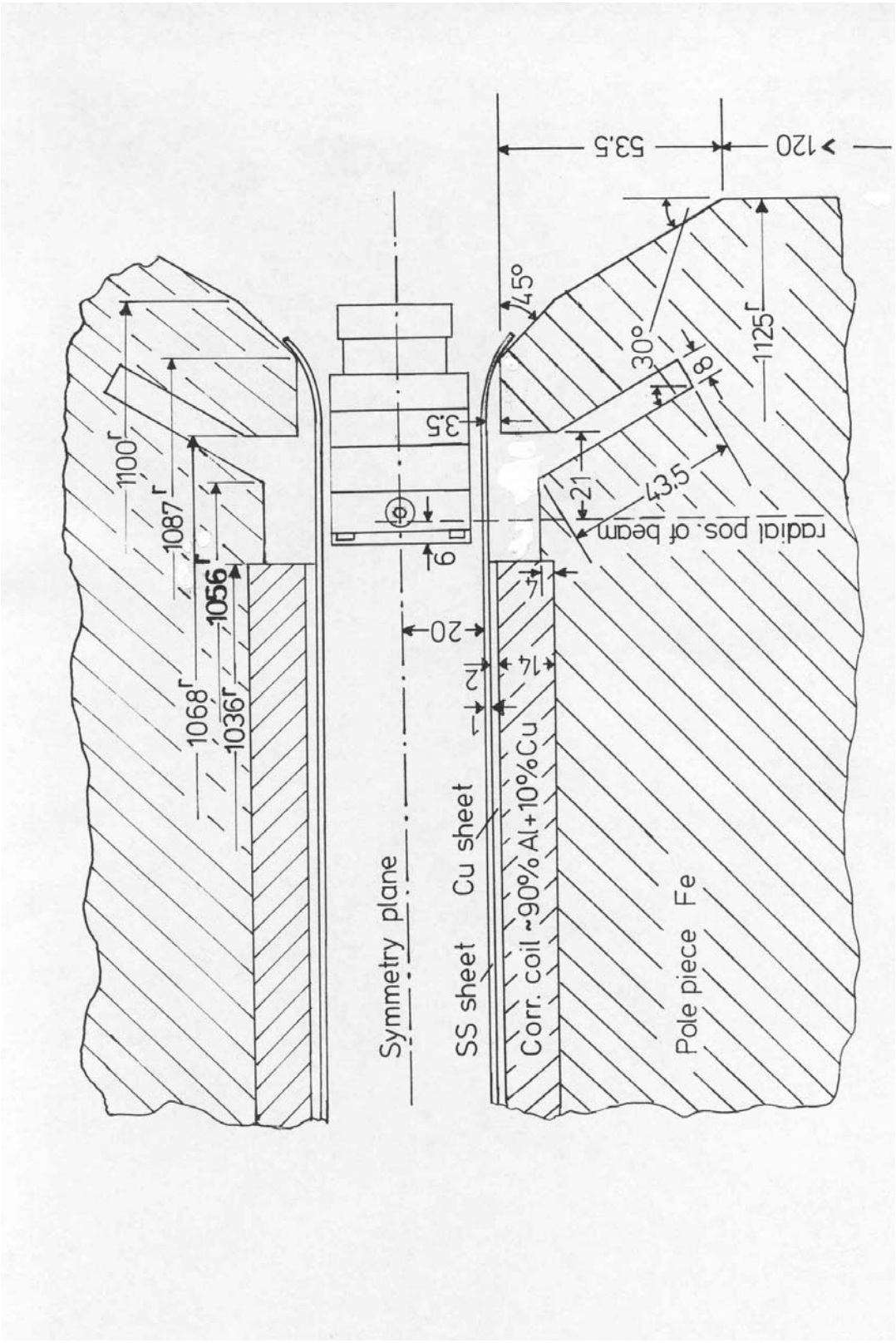

Figure 2-2 Target in irradiation position near cyclotron pole pieces

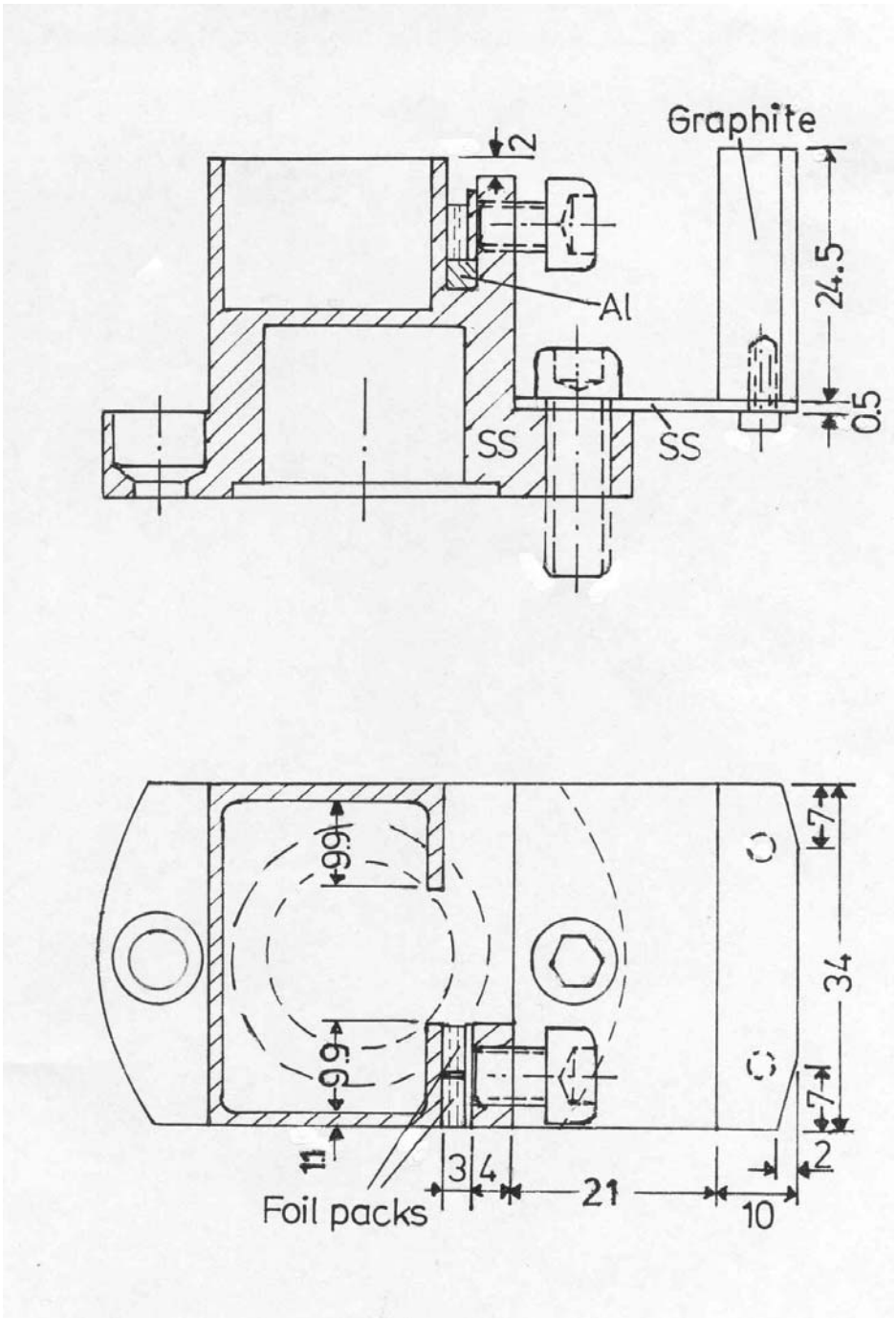

Figure 2-3 Empty target hood with attached graphite beamstop

Dimensions not specified are the same as the corresponding ones in Fig. 2-1

gent) beam. Moreover, the net electric beam current on such a target is zero, so that a separate beam stop is required as an electrode for measuring the current. On the other hand, the container lid can be omitted, as it does not influence the neutron production. For the beam stop material, graphite was selected to minimize neutron production on it. To further reduce the registration of any neutrons from the beam stop by the activation foils, the beam stop was placed as far downstream as space permitted. The resulting design is shown in Fig. 2-3. The two foil irradiation positions shown are denoted Near (i.e., closer to the forward beam direction) and Far.

Fig. 2-4 is a photograph of one of the lithium target hoods (target A) and the empty target hood before mounting the graphite beam stop, viewed from the upstream (beam incidence) side. Fig. 2-5 is the same viewed from the downstream side.

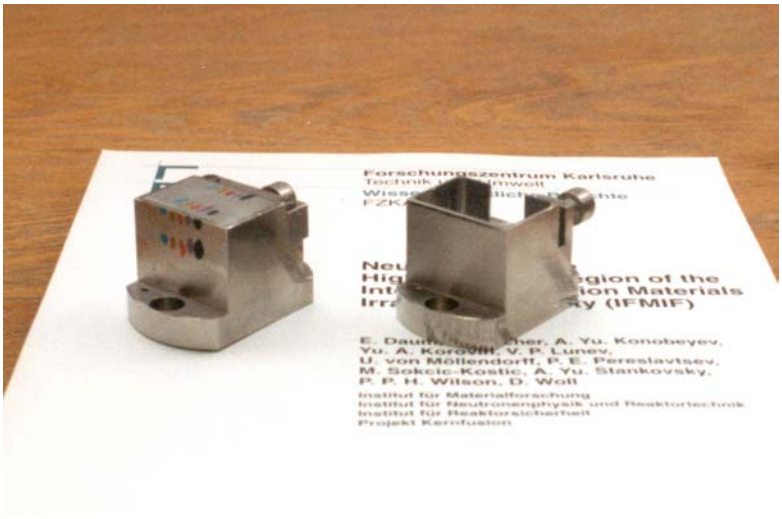

Figure 2-4 Lithium target hood A and empty target hood, seen from upstream side

Figure 2-5 Lithium target hood A and empty target hood, seen from downstream side

2.4 Irradiation procedures

One of the three lithium-filled targets (target A) was used to try what beam current could safely be used with respect to heat removal. The target was irradiated at 1, 2, 3, . . . μA for about 15 minutes each, and removed for inspection each time. After the 7 μA irradiation, a bubble-like structure had become visible on the steel container at the spot where the beam impinged. Thereupon, the current of 3 μA was adopted as safe for the subsequent irradiations, which were made with a fresh target (target B).

The beam spot on the target wall was roughly 2.5 mm in diameter. Its centre was situated 5.5 mm from the edge near the welded lid (i.e., the upper edge in the upper part of Fig. 2-1) and 15 mm from the upper edge in the lower part of Fig. 2-1, i.e., about 2 mm above the horizontal symmetry plane shown in Fig. 2-2. It is one of the disadvantages of an internal as opposed to an external target, that a vertical adjustment of the beam position is not possible.

In Figs. 2-4 and 2-5, rows of (coloured) spots are seen on lithium target A. These are temperature indicating paints, intended to give some information on the temperature distribution on the container surface. However, as mentioned above, the local heat deposition at the beam spot rather than any volume heating turned out to be the limiting effect.

For the neutron spectrum and yield measurement on target B, three irradiations of 20 min, 2 h and 12 h duration were performed, each time with different, suitable sets of dosimetry foils in the two positions. Afterwards, the four structural material samples were placed together as a stack, including monitor foils and, where required, stopping foils [Mö02], in the Centre position and irradiated for 2 h. The empty target was irradiated for 5 h. It had packs of dosimetry foils in the two provided positions (see Fig. 2-3).

In all irradiations, the beam current was registered by a calibrated current-to-frequency converter and a repeating scaler (Ortec model 974) controlled and read out by a personal computer. The time resolution, i.e. the interval of current integration, was selected at 60 seconds. This was sufficient in view of the shortest halflife of interest, which was 9.5 minutes (the $^{27}Al(n,p)^{27}Mg$ dosimetry reaction).

3 NEUTRON FIELD

3.1 General remarks

The neutron spectrum and yield measurement had to rely on activation foil dosimetry, because other techniques were not available in the given experimental situation at the cyclotron (cf. Ref.[Mö02] for details). This method is inherently of limited precision, as it requires the numerical deconvolution of the spectrum from a set of measured reaction rates. On the other hand, its advantage, at least in view of the subsequent material activation experiments, is that it measures the spectrum and yield averaged just over the transverse area of the foil sandwich. As long as a material activation sample has the same dimensions and position, it will be exposed to the same neutron field. If the neutron field on such a sample would have to be inferred, e.g., from the spectrum measured by a scintillation detector at some larger distance from the neutron source, the spatial distribution of neutron generation in the target would introduce some systematic uncertainty.

3.2 Spectrum and gross yield

The spectrum measurement was described earlier [Ma00]. Table 3-1 is a list of the dosimetry reactions used. Table 3-2 gives the 45-group energy structure adopted. Tables 3-3 and 3-4 give the spectra obtained in the Centre and Side positions respectively, without correction for the neutrons produced in the steel wall. This Centre spectrum is to be used, e.g., in analyzing the structural material activation measurement. Graphs of the spectra in energy representation are given in Fig. 3-1. The uncertainty of either spectrum, referred to calculations of threshold neutron reaction rates, is estimated at ±10% [Ma00].

Table 3-1 List of dosimetry reactions used in determining the neutron spectra

Reactions marked * were also used in the empty target measurement

Reaction	Threshold (MeV)	Half life
$^{27}Al(n,p)^{27}Mg$	1.9	9.458 min
$^{27}Al(n,\alpha)^{24}Na$ *	3.2	14.959 h
$^{55}Mn(n,2n)^{54}Mn$ *	10.4	312.12 d
$^{nat}Fe(n,x)^{54}Mn$	0	312.12 d
$^{nat}Fe(n,x)^{56}Mn$	3.0	2.5785 d
$^{59}Co(n,2n)^{58}Co$	10.6	70.82 d
$^{59}Co(n,3n)^{57}Co$	19.4	271.79 d
$^{59}Co(n,p)^{59}Fe$	0.8	44.503 d
$^{59}Co(n,\alpha)^{56}Mn$	0	2.5785 h
$^{nat}Ni(n,x)^{58}Co$ *	0	70.82 d
$^{nat}Ni(n,x)^{57}Co$ *	8.3	271.79 d
$^{nat}Ni(n,x)^{57}Ni$ *	12.4	35.60 h
$^{89}Y(n,2n)^{88}Y$ *	11.6	106.65 d
$^{89}Y(n,3n)^{87m+g}Y$ *	21.1	79.8 h
$^{93}Nb(n,2n)^{92m}Nb$ *	8.9	10.15 d
$^{115}In(n,n')^{115m}In$ *	0.3	4.486 h
$^{169}Tm(n,2n)^{168}Tm$ *	8.1	93.1 d
$^{169}Tm(n,3n)^{167}Tm$ *	15.0	9.25 d
$^{169}Tm(n,4n)^{166}Tm$ *	23.7	7.70 h
$^{197}Au(n,2n)^{196m}Au$	8.7	9.7 h
$^{197}Au(n,2n)^{196m+g}Au$	8.1	6.183 d
$^{197}Au(n,3n)^{195m}Au$	14.8	186.09 d
$^{197}Au(n,4n)^{194m}Au$	23.2	38.02 h
$^{209}Bi(n,3n)^{207}Bi$	14.4	31.55 a
$^{209}Bi(n,4n)^{206}Bi$	22.6	6.243 d
$^{209}Bi(n,5n)^{205}Bi$	29.6	15.31 d
$^{209}Bi(n,6n)^{204}Bi$	38.0	11.22 h

Table 3-2 Energy group boundaries in MeV

5.6230e+01	5.0120e+01	4.4670e+01	3.9810e+01	3.5480e+01	3.1620e+01
2.8180e+01	2.5120e+01	2.2390e+01	1.9950e+01	1.7780e+01	1.5850e+01
1.4130e+01	1.2590e+01	1.1220e+01	1.0000e+01	8.9130e+00	7.9430e+00
7.0790e+00	6.3100e+00	5.6230e+00	5.0120e+00	4.4670e+00	3.9810e+00
3.5480e+00	3.1620e+00	2.8180e+00	2.5120e+00	2.2390e+00	1.9950e+00
1.7780e+00	1.5850e+00	1.4130e+00	1.2590e+00	1.1220e+00	1.0000e+00
8.9130e-01	7.9430e-01	7.0790e-01	6.3100e-01	5.6230e-01	5.0120e-01
4.4670e-01	3.9810e-01	3.5480e-01	3.1620e-01		

Table 3-3 Average specific neutron flux in each energy group on a 5x5 mm^2 sample at the Centre position in units of 10^{18} n cm^{-2} s^{-1} μA^{-1}

6.7686e-11	3.5015e-10	5.1813e-10	8.0628e-10	1.6659e-09	2.9815e-09
4.9779e-09	6.9106e-09	7.9884e-09	8.5388e-09	8.2623e-09	7.5668e-09
6.8311e-09	6.2134e-09	5.6306e-09	5.0988e-09	4.7480e-09	4.5948e-09
4.6480e-09	4.7237e-09	4.5229e-09	4.1866e-09	3.8766e-09	3.6884e-09
3.6426e-09	3.5827e-09	3.4030e-09	3.1996e-09	3.0639e-09	2.8524e-09
2.4664e-09	1.9819e-09	1.6686e-09	1.4985e-09	1.3904e-09	1.2480e-09
1.0952e-09	1.0311e-09	9.6038e-10	8.7831e-10	8.2466e-10	8.1234e-10
8.9370e-10	8.4834e-10	7.5798e-10			

Table 3-4 Average specific neutron flux in each energy group on a 5x5 mm^2 sample at the Side position in units of 10^{18} n cm^{-2} s^{-1} μA^{-1}

2.0672e-11	8.9209e-11	1.3389e-10	2.2602e-10	3.2048e-10	4.6389e-10
6.9000e-10	8.9603e-10	1.0784e-09	1.2154e-09	1.3467e-09	1.3447e-09
1.2476e-09	1.1747e-09	1.1559e-09	1.1416e-09	1.1289e-09	1.1631e-09
1.1617e-09	1.1260e-09	1.0928e-09	1.0459e-09	9.6840e-10	8.9323e-10
8.3097e-10	7.6842e-10	7.2199e-10	6.8905e-10	6.5118e-10	6.1695e-10
5.7842e-10	5.4846e-10	5.1327e-10	4.7480e-10	4.3642e-10	3.9804e-10
3.6028e-10	3.4501e-10	3.2054e-10	2.6987e-10	2.4732e-10	2.3578e-10
2.1213e-10	1.9804e-10	1.6694e-10			

Summation of the specific group flux values of Tables 3-3 and 3-4 results in total yields (specific neutron flux densities averaged over the respective region of solid angle covered) of 1.478×10^{11} n cm^{-2} s^{-1} μA^{-1} in the Centre position and 3.071×10^{10} n cm^{-2} s^{-1} μA^{-1} in the Side position.

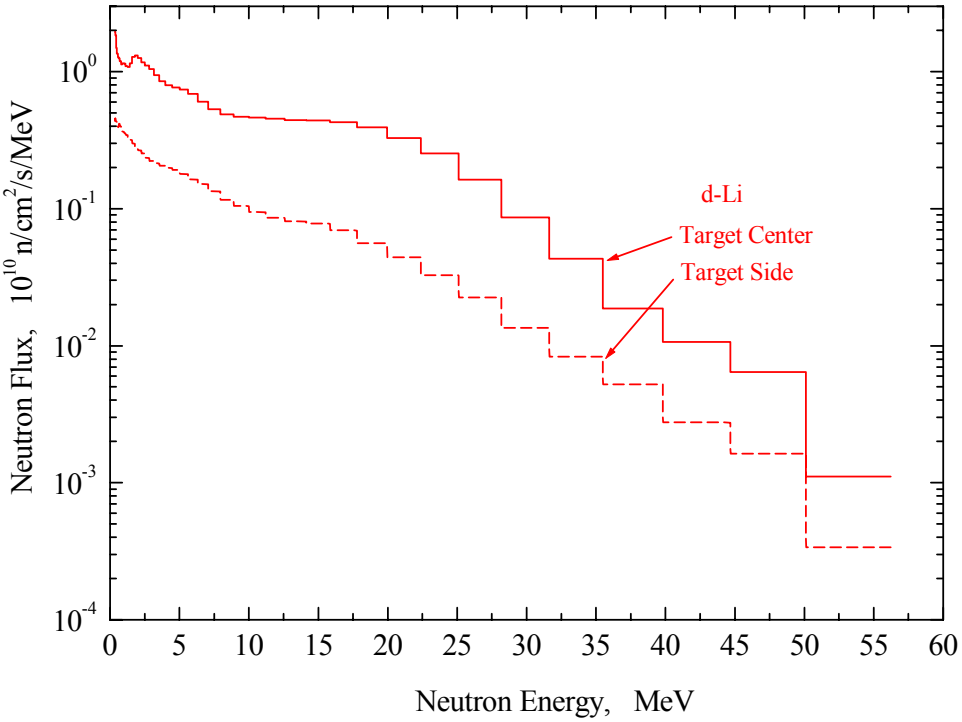

Fig. 3-1 'Centre' and 'Side' neutron spectra

3.3 Yield corrected for neutrons from target container

As mentioned in Ref.[Ma00], the dosimetry reaction rates measured in the Near position of the empty target are about 10...20% of those measured in the Side position of the Li target (these two positions are roughly equivalent in geometry). The variety of dosimetry reactions used was less than for the filled target, and no attempt was made to unfold the shape of the spectrum. However, it can be assumed to be similar to the spectrum from the filled target, because deuteron stripping certainly is the predominant reaction mechanism in either case. Assuming therefore, with some further simplification, that

- both the spectral shape and the angular distribution of 'container neutrons' are the same as for d+Li neutrons,
- the yield of 'container neutrons' is (15±5)% of the total yield given above, and
- the ±10% uncertainty of the spectrum is valid also for the total yield,

we obtain for the neutron yield from an open-surface lithium target (as in IFMIF) irradiated by 40 MeV deuterons

$$\mathbf{1.26\times10^{11}\ n\ cm^{-2}s^{-1}\mu A^{-1}} \quad \pm 12\%$$

in the Centre position and

$$\mathbf{2.61\times10^{10}\ n\ cm^{-2}s^{-1}\mu A^{-1}} \quad \pm 12\%$$

in the Side position. The quantity interesting for IFMIF analyses, the total specific neutron yield integrated over all emission directions, in neutrons per microampere or neutrons per deuteron can be inferred by fitting suitable model calculations to these integral values.

4 RADIOACTIVITY PRODUCTION IN THE TARGET

4.1 General remarks

Pure lithium irradiated by deuterons of $E_d \leq 40$ MeV will produce two radionuclides of practical importance to the operation of IFMIF: tritium (by reactions such as, e.g., $^{7}Li(d,t)^{6}Li$) and beryllium-7 (by, e.g., $^{6}Li(d,n)^{7}Be$). The half lives of H-3 and Be-7 are 12.3 a and 53.3 d respectively. In addition there will be, due to two-step reactions, a small yield of beryllium-10, a very long lived pure β ray emitter ($T_{1/2} = 1.6\times10^{6}$ a). Any other radionuclides that can originate from deuterons and lithium have half lives of seconds or milliseconds. The present experiment provided an opportunity to measure the H-3 and Be-7 yields.

One important difference between IFMIF and the present simulation experiment is the steel target wall on the beam entrance side. To correct for the effect of deuterons absorbed there, we use similar assumptions as made in Section 3.3, i.e., we assume that only (85±5)% of the beam deuterons have reached the lithium.

4.2 Tritium measurement and result

For the tritium measurement, both of the irradiated lithium targets (see sect. 2.4) were subjected to a procedure which is well established, but was nevertheless first tried in a 'dry' run using the spare, non-irradiated target. The technique consisted in releasing the tritium by heating the target to several hundred °C in a quartz tube through which a gas stream of 95% Ar + 5% H_2 was flowing at 50 ml/min. The gas was subsequently oxidized in passing through a CuO bed. The resulting H_2O+HTO gas was absorbed in a molecular sieve. The molecular sieve was periodically changed and eluted with water. This water was then analyzed for tritium in an automated liquid scintillation system (Beckman Instruments LS 6000TA).

The result after correcting for decay, expressed in produced tritons per 100 deuterons incident on the steel-clad target, is 2.43 in target A and 2.30 in target B, with an estimated uncertainty of ± 5% in either measurement. Averaging these and applying the correction for the target steel wall mentioned above, the final result is

(2.78 ± 7%) tritons per 100 deuterons incident on the lithium

which corresponds to

(6.85 g ± 7%) tritium per IFMIF full power year.

If all the tritium were produced from Li-7, the effective production cross section per Li-7 atom averaged over deuteron energy (0...40 MeV) would be

297 mb ± 7%**.**

4.3 Beryllium-7 measurement and result

After a cooling time of about 100 days to decrease the considerable activity induced in the steel, and before the lithium targets were destroyed for determining the tritium content, the 478 keV γ ray line from target B was measured with a γ spectrometer that employs a coaxial, 25% efficiency high purity germanium crystal [Mö02]. The spectrometer, which usually is employed for analysing much weaker samples, had to be reduced in counting efficiency for this measurement by using a lead collimator in front of the detector. Two separate sets of measurements were taken with collimators of different dimensions, a 50 mm thick slab with a 10 mm dia. bore and a 30 mm thick slab with a 12 mm dia. bore. The spectrometer was re-calibrated in either case with a Eu-152 γ ray source. Either collimator had a different position in front of the detector, but always eccentric with respect to the detector axis to avoid the detector centre with its reduced efficiency (see Fig. 4-1). The distance between radiation source and collimator was 65 cm. The correct source position was found by seeking, in several series of short measurements, the maximum 487 keV counting rate as a function of source position along a horizontal or vertical scale at right angles to the collimator axis.

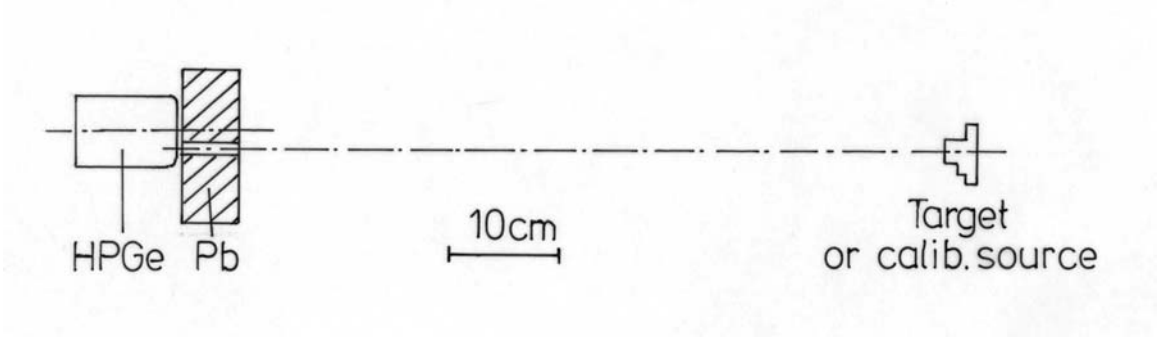

Figure 4-1 Measurement of Be-7 γ radiation

The measurement constitutes a comparison of the unknown Be-7 activity to the known activity of the calibration source. As the Eu-152 calibration source is practically point shaped, the unknown spatial distribution of the Be-7 within the Li target of finite size causes a small systematic uncertainty in view of shadowing effects of the collimator. For a homogeneous distribution, a counting rate reduction of <5% compared to the point-source case is expected with

the narrower collimator. Experimentally, no systematic difference between Be-7 activities measured with the two collimators was found.

The emitted γ radiation is reduced by absorption in the steel case by about 8%. The γ ray absorption within the lithium, assuming all radiation to be emitted at a depth of 7 mm (half the lithium thickness in the direction of measurement), amounts to about 4%. Applying these corrections as well as the one for deuteron loss in the steel wall (see above), the result for the Be-7 yield is

(0.322 ± 12%**) Be-7 atoms per 100 deuterons incident on the lithium**

corresponding to

(1.85 g ± 12%**) Be-7 per IFMIF full power year.**

If all the Be-7 were produced by the $^{6}Li(d,n)^{7}Be$ reaction, the effective production cross section per Li-6 atom averaged over deuteron energy (0...40 MeV) would be

426 mb ± 12%**.**

The 12% uncertainty derives from the scatter of several Be-7 and calibration measurements and the uncertainties of the corrections.

5 NEUTRON-INDUCED ACTIVATION OF STRUCTURAL MATERIALS

5.1 General remarks

Given the high energies of IFMIF neutrons, activation in the IFMIF spectrum is even more complex than in a fusion neutron spectrum. Products of nuclear reactions having threshold energies as high as 28 MeV, e.g., many (n,3n) reactions, were observed in our structural material samples. In the neutron spectrum measurement, dosimetry reactions with thresholds even up to 38 MeV (see Table 3-1) were utilized. Thus, a multitude of radionuclides can result simultaneously from irradiating one pure target nuclide, and, inversely, in a multi-isotope element or, e.g., an alloy such as a chromium-nickel steel, one given product nuclide can originate via different pathways from different target nuclides simultaneously. (The term pathway, as opposed to reaction channel, denotes the complete process that leads from the target nuclide to the product nuclide. A pathway comprises at least one neutron-induced reaction channel, but it may be a chain of several reactions and radioactive decays.)

Activation experiments of this kind are denoted 'integral', because the measured quantity is not the cross section $\sigma(E_n)$ but the reaction rate $\int \varphi(E_n)\sigma(E_n)\mathrm{d}E_n$, where $\varphi(E_n)$ is the spectral or differential neutron flux density. More loosely speaking, they are ‘integral’ also in the sense that multi-pathway production of the same product is important in many cases.

In the IFMIF neutron spectrum, similar as in fusion reactor neutron spectra, the (n,γ) or neutron capture reactions are, generally, not as dominating as they are in activation in fission reactors.

The fast charged particles emitted from reactions can induce further reactions on nuclei present in the irradiated material. If such a secondary reaction results, e.g., in neutron emission, a target of atomic number Z can be transmuted into a product nuclide with atomic number Z+1 or Z+2, which is not possible with neutron induced reactions. The importance of these 'sequential charged-particle reactions' for neutron-induced activation was noted by Cierjacks et al.[Ci93], who also introduced a concept for describing them within nuclear data libraries by pseudo cross sections for incident neutrons.

5.2 Samples and activation parameters

The activation experiment has basically been described in Refs.[Mö98, Mö99, Ma00, Mö00]. The structural material samples were of square shape and 5mm by 5mm in size, with thicknesses ranging from 0.3 to 0.4 mm. The four samples, SS-316 steel, F82H steel, pure vana-

dium, and V-4Ti-4Cr alloy, were attached jointly, forming a stack, to the lithium target in the same position as the Centre foil stack in the neutron spectrum measurement. Aluminium fluence monitor foils interspersed with the four samples served to determine the relative fluence decrease across the stack thickness, by measuring and comparing their Na-24 activities induced by the $^{27}Al(n,\alpha)$ reaction. The activation parameters are given in Table 5-1 and the elemental compositions, as analyzed at JAERI, in Table 5-2.

In order to account for neutron flux variations during the irradiation, the beam current was recorded in a time dependent way, and halflife dependent correction factors were calculated from these data (see Ref.[Mö02] for details). However, the correction factor differs from unity by less than 0.004 throughout this experiment, so that the correction can be neglected.

Table 5-1 Activation parameters

Material	Neutron flux density, Φ (cm^{-2} s^{-1})	Activation time, T_A (s)
SS-316	4.10 E11	7525
F82H	4.14 E11	
V alloy	4.22 E11	
V pure	4.27 E11	

Table 5-2 Compositions of samples in weight%

Element	SS-316	F82H	V alloy	V pure
B	<0.0002	0.0002	<0.0005	<0.0005
C		0.09	0.0045	0.0027
N		0.008	0.011	0.013
O			0.037	0.041
Mg			<0.001	<0.001
Al	<0.05	0.003	0.020	0.025
Si	0.4	0.11	0.034	0.017
P		0.002	0.003	<0.003
S		0.002	0.001	<0.001
Ti	<0.15	0.01	**4.1**	
V		0.16	**balance**	**balance**
Cr	**17.5**	**7.70**	**3.9**	
Mn	1.8	0.16		
Fe	**balance**	**balance**	0.021	0.016
Co	0.03	0.005		
Ni	**12.3**	0.02		
Cu	<0.1	0.01	<0.005	<0.005
Nb	<0.005	0.0001	0.0087	0.004
Mo	**2.5**	0.003	<0.005	<0.005
Ta		0.02		
W		**1.95**		

5.3 Gamma spectrometry and results

Gamma spectrometry on the activated samples was performed at six (partly seven) different cooling times, ranging from about 1 hour to 150 days. The equipment and procedure were largely those described in Ref.[Mö02], however, the analysis of the spectra was performed at Tokai-mura. The results A_{sp}, specific activities in Becqerels per kilogram of sample material at each cooling time T_c (the time elapsed from end of activation), are given in Tables 5-3 to 5-7.

Table 5-3 SS-316, experimental results, $Z \leq 28$

Product	$T_{½}$ ≈	T_c = 5965 s		T_c = 18 848 s		T_c = 93 333 s		T_c = 178 860 s	
		A_{sp}	±	A_{sp}	±	A_{sp}	±	A_{sp}	±
		Bq/kg	%	Bq/kg	%	Bq/kg	%	Bq/kg	%
Sc-46	84 d							**5.33 E4**	54
Sc-48	44 h					**3.37 E6**	13	**1.57 E6**	9
V-48	16 d					**1.04 E6**	14	**1.08 E6**	9
Cr-48	22 h							**1.05 E5**	25
Cr-49	42 min	**2.22 E8**	35						
Cr-51	28 d			**3.14 E8**	27	**2.91 E8**	5	**2.78 E8**	5
Mn-52g	5.6 d			**1.14 E7**	40	**1.01 E7**	6	**7.72 E6**	5
Mn-54	312 d			**2.68 E7**	33	**1.82 E7**	5	**1.73 E7**	5
Mn-56	2.6 h	**2.61E10**	5	**9.60 E9**	5	**3.83 E7**	5		
Fe-52	8.3 h					**3.41 E5**	50		
Fe-59	45 d							**3.50 E5**	18
Co-55	18 h					**2.30 E6**	16	**5.81 E5**	10
Co-56	77 d					**2.54 E6**	21	**2.82 E6**	5
Co-57	272 d			**2.19 E7**	39	**2.08 E7**	6	**2.03 E7**	5
Co-58g	71 d			**5.71 E7**	16	**7.18 E7**	5	**7.36 E7**	5
Co-60	5.3 a							**2.35 E5**	15
Co-61	1.7 h	**1.04 E8**	34						
Ni-56	6.1 d					**1.32 E6**	17	**1.21 E6**	7
Ni-57	36 h	**2.59 E8**	27	**2.49 E8**	23	**1.72 E8**	21	**9.44 E7**	21

Table 5-3 continued

Product	$T_{½}$ ≈	T_c = 432 539 s		T_c = 2 520 240 s		T_c = 12 962 640 s	
		A_{sp}	±	A_{sp}	±	A_{sp}	±
		Bq/kg	%	Bq/kg	%	Bq/kg	%
Sc-46	84 d			**5.72 E4**	13	**2.20 E4**	18
Sc-48	44 h	**6.55 E5**	14				
V-48	16 d	**9.03 E5**	9	**3.41 E5**	6		
Cr-48	22 h						
Cr-49	42 min						
Cr-51	28 d	**2.58 E8**	5	**1.38 E8**	5	**6.83 E6**	5
Mn-52g	5.6 d	**5.38 E6**	5	**2.74 E5**	6		
Mn-54	312 d	**1.71 E7**	5	**1.59 E7**	5	**1.22 E7**	5
Mn-56	2.6 h						
Fe-52	8.3 h						
Fe-59	45 d			**2.33 E5**	10	**3.21 E4**	39
Co-55	18 h						
Co-56	77 d	**2.67 E6**	7	**2.12 E6**	5	**7.22 E5**	5
Co-57	272 d	**2.01 E7**	5	**1.91 E7**	5	**1.41 E7**	5
Co-58g	71 d	**7.13 E7**	5	**5.53 E7**	5	**1.70 E7**	5
Co-60	5.3 a	**2.88 E5**	27	**2.60 E5**	6	**2.23 E5**	6
Co-61	1.7 h						
Ni-56	6.1 d	**9.21 E5**	11				
Ni-57	36 h	**2.70 E7**	21				

Table 5-4 SS-316, experimental results, $Z > 28$

Product	$T_{½}$ ≈	T_c = 5965 s		T_c = 18 848 s		T_c = 93 333 s		T_c = 178 860 s	
		A_{sp}	±	A_{sp}	±	A_{sp}	±	A_{sp}	±
		Bq/kg	%	Bq/kg	%	Bq/kg	%	Bq/kg	%
Y-87m	13 h							**1.25 E5**	28
Y-87g	80 h							**1.80 E5**	19
Y-88	107 d								
Zr-86	17 h							**1.16 E5**	23
Zr-88	83 d								
Zr-89g	78 h					**1.71 E6**	18	**1.29 E6**	5
Zr-97	17 h							**5.44 E6**	21
Nb-90g	15 h					**7.55 E6**	8	**1.73 E6**	6
Nb-92m	10 d					**1.39 E6**	31	**1.82 E6**	11
Nb-95g	35 d					**5.90 E5**	37	**4.88 E5**	8
Nb-95m	87 h							**9.39 E5**	13
Nb-96	23 h					**5.36 E6**	9	**2.28 E6**	5
Mo-90	5.7 h							**1.45 E4**	55
Mo-93m	6.9 h					**1.85 E6**	18	**7.26 E4**	35
Mo-99	66 h					**4.84 E7**	7	**3.21 E7**	6
Tc-99m	6.0 h			**5.69 E7**	16	**4.45 E7**	5	**3.08 E7**	5

Table 5-4 continued

Product	$T_{½}$ ≈	T_c = 432 539 s		T_c = 2 520 240 s		T_c = 12 962 640 s	
		A_{sp}	±	A_{sp}	±	A_{sp}	±
		Bq/kg	%	Bq/kg	%	Bq/kg	%
Y-87m	13 h						
Y-87g	80 h						
Y-88	107 d					**1.05 E4**	34
Zr-86	17 h						
Zr-88	83 d			**2.28 E4**	60		
Zr-89g	78 h	**7.68 E5**	11				
Zr-97	17 h						
Nb-90g	15 h						
Nb-92m	10 d	**1.79 E6**	9	**2.89 E5**	7		
Nb-95g	35 d	**5.36 E5**	17	**3.29 E5**	6	**4.09 E4**	19
Nb-95m	87 h						
Nb-96	23 h	**3.37 E5**	25				
Mo-90	5.7 h						
Mo-93m	6.9 h						
Mo-99	66 h	**1.57 E7**	7				
Tc-99m	6.0 h	**1.54 E7**	5	**2.24 E4**	47		

Table 5-5 F82H, experimental results

Product	$T_{½}$ ≈	T_c = 4173 s		T_c = 18 011 s		T_c = 92 043 s		T_c = 158 665 s	
		A_{sp}	±	A_{sp}	±	A_{sp}	±	A_{sp}	±
		Bq/kg	%	Bq/kg	%	Bq/kg	%	Bq/kg	%
Sc-46	84 d							**4.13 E4**	44
Sc-47	3.4 d					**7.17 E5**	20	**6.78 E5**	12
Sc-48	44 d					**2.06 E6**	11	**1.35 E6**	5
V-48	16 d					**3.53 E5**	32	**5.57 E5**	16
Cr-48	22 h							**7.81 E4**	30
Cr-49	42 min	**3.14 E8**	28						
Cr-51	28 d					**1.42 E8**	5	**1.37 E8**	5
Mn-52g	5.6 d					**1.13 E7**	6	**1.02 E7**	5
Mn-54	312 d					**1.80 E7**	5	**1.76 E7**	5
Mn-56	2.6 h	**4.08 E10**	5	**1.45 E10**	5	**5.71 E7**	6	**2.70 E5**	11
Fe-52	8.3 h					**5.39 E5**	22	**1.09 E5**	18
Co-55	18 h					**1.01 E6**	22	**6.65 E5**	9
Co-56	77 d							**7.52 E5**	8
Co-57	272 d								
Co-58g	71 d							**1.74 E5**	17
Co-60	5.3 a								
Ni-57	36 h							**2.51 E5**	24
Tc-99m	6.0 h							**4.57 E4**	40
Ta-182	114 d								
Ta-183	5.0 d					**1.05 E6**	20	**1.02 E6**	18
Ta-184	8.7 h					**7.10 E5**	44	**9.81 E4**	52
W-187	23.7 h					**4.60 E6**	17	**2.83 E6**	7

Table 5-5 continued

Product	$T_{½}$ ≈	T_c = 424 416 s		T_c = 2 922 060 s		T_c = 13 036 200 s	
		A_{sp}	±	A_{sp}	±	A_{sp}	±
		Bq/kg	%	Bq/kg	%	Bq/kg	%
Sc-46	84 d			**3.56 E4**	10	**1.44 E4**	15
Sc-47	3.4 d	**3.59 E5**	20				
Sc-48	44 d	**5.00 E5**	10				
V-48	16 d	**3.55 E5**	13	**1.25 E5**	6		
Cr-48	22 h						
Cr-49	42 min						
Cr-51	28 d	**1.27 E8**	5	**6.00 E7**	4	**3.31 E6**	5
Mn-52g	5.6 d	**7.13 E6**	5	**1.73 E5**	6		
Mn-54	312 d	**1.78 E7**	5	**1.65 E7**	4	**1.27 E7**	4
Mn-56	2.6 h						
Fe-52	8.3 h						
Co-55	18 h						
Co-56	77 d	**7.20 E5**	13	**5.74 E5**	5	**2.04 E5**	7
Co-57	272 d			**3.91 E4**	13	**3.69 E4**	16
Co-58g	71 d	**1.68 E5**	28	**1.12 E5**	7	**3.76 E4**	18
Co-60	5.3 a			**1.40 E4**	16	**7.05 E3**	30
Ni-57	36 h						
Tc-99m	6.0 h						
Ta-182	114 d	**1.31 E5**	13				
Ta-183	5.0 d	**7.88 E5**	29				
Ta-184	8.7 h						
W-187	23.7 h						

Table 5-6 V-Alloy, experimental results

Product	$T_{½}$ ≈	T_c = 5477 s		T_c = 17 189 s		T_c = 90 710 s	
		A_{sp}	±	A_{sp}	±	A_{sp}	±
		Bq/kg	%	Bq/kg	%	Bq/kg	%
Ca-47	4.5 d						
Sc-43	3.9 h	**3.85 E7**	26				
Sc-44g	3.9 h	**1.92 E7**	21	**1.62 E7**	18		
Sc-44m	2.4 d						
Sc-46	84 d	**4.00 E6**	72	**6.05 E6**	47	**4.09 E6**	27
Sc-47	3.4 d	**4.87 E8**	5	**5.36 E8**	5	**4.46 E8**	5
Sc-48	44 d	**9.72 E8**	5	**1.04 E9**	5	**7.30 E8**	5
V-48	16 d						
Cr-49	42 min	**5.89 E7**	15				
Cr-51	28 d	**8.00 E7**	37	**6.98 E7**	27	**8.74 E7**	16
Mn-52g	5.6 d						
Nb-92m	10 d						

Product	$T_{½}$ ≈	T_c = 417 962 s		T_c = 2 254 080 s		T_c = 13 341 780 s	
		A_{sp}	±	A_{sp}	±	A_{sp}	±
		Bq/kg	%	Bq/kg	%	Bq/kg	%
Ca-47	4.5 d	**1.09 E6**	18	**5.06 E4**	15		
Sc-43	3.9 h						
Sc-44g	3.9 h						
Sc-44m	2.4 d	**4.43 E5**	28				
Sc-46	84 d	**4.97 E6**	6	**4.40 E6**	4	**1.47 E6**	4
Sc-47	3.4 d	**2.05 E8**	5	**1.92 E6**	7		
Sc-48	44 d	**1.70 E8**	5	**3.08 E4**	11		
V-48	16 d			**2.12 E6**	4	**1.94 E4**	24
Cr-49	42 min						
Cr-51	28 d	**6.16 E7**	5	**3.55 E7**	4	**1.38 E6**	5
Mn-52g	5.6 d			**9.50 E3**	25		
Nb-92m	10 d			**3.85 E4**	10		

Table 5-7 V-Pure, experimental results

Product	$T_{½}$ ≈	T_c = 4983 s		T_c = 16 396 s		T_c = 90 001 s	
		A_{sp}	±	A_{sp}	±	A_{sp}	±
		Bq/kg	%	Bq/kg	%	Bq/kg	%
Ca-47	4.5 d						
Sc-46	84 d						
Sc-47	3.4 d	**4.99 E8**	5	**4.80 E8**	5	**3.98 E8**	5
Sc-48	44 d	**9.38 E8**	5	**9.01 E8**	5	**6.56 E8**	5
V-48	16 d						
Cr-51	28 d						
Nb-92m	10 d						

Product	$T_{½}$ ≈	T_c = 412 474 s		T_c = 3 100 500 s		T_c = 13 146 900 s	
		A_{sp}	±	A_{sp}	±	A_{sp}	±
		Bq/kg	%	Bq/kg	%	Bq/kg	%
Ca-47	4.5 d	**1.11 E6**	18	**4.53 E3**	36		
Sc-46	84 d	**3.01 E6**	8	**2.31 E6**	4	**8.47 E5**	4
Sc-47	3.4 d	**1.84 E8**	5	**2.08 E5**	7		
Sc-48	44 d	**1.52 E8**	4				
V-48	16 d	**6.10 E6**	31	**1.33 E6**	4	**9.14 E3**	33
Cr-51	28 d	**1.05 E7**	10	**4.33 E6**	4	**2.33 E5**	11
Nb-92m	10 d			**6.53 E3**	27		

6 CONCLUSIONS

In the described nuclear simulation experiment for IFMIF, several quantities were measured — the neutron yield and spectrum, the production rates of the long lived radionuclides tritium and beryllium-7 in the lithium target, and production rates of many γ emitting radionuclides generated in different structural materials under irradiation in this neutron field. All the quantitative results, with experimental uncertainties, and all relevant parameters of the experiment are given in this report, so that it forms a basis for future calculations that will help to benchmark or validate nuclear data libraries or calculational methods.

The neutron yield results represent integrals over two specific regions of solid angle, not the total of produced neutrons. Their generalization to the full solid angle of interest (in case of IFMIF, essentially the 2π sr forward hemisphere) will have to be made using Monte Carlo calculations with detailed modelling of the target and deuteron beam. The M^{c}Delicious code[Si02] is a suitable tool for this. Of course, also the measured neutron spectra apply, strictly speaking, only to those two experimental solid angle regions.

The tritium and Be-7 production results, beyond allowing a benchmarking of calculations, are immediately applicable to the IFMIF design.

The neutron-induced activation results represent the first integral benchmark experiment for the Intermediate Energy Activation File (IEAF) [Mö00, Ko01] and any similar libraries. The results obtained for vanadium have been useful already in testing the respective IEAF-2001 data [Fi02].

Acknowledgements

The authors are grateful to Dr. J. Konys for his advice and proposals about the design and choice of material for the target container. The precision machining of the target hoods was done by Mr. W. Gorenflo. Ms. Z. Voss and Mr. O. Wedemeyer kindly and carefully performed the filling of these with lithium. The experiment could not have been performed without the efficient support by Mr. J. Möllenbeck and the operation crew at the cyclotron department. We thank JAERI Tokai-mura and, in particular, Dr. Y. Ikeda for enabling the collaboration under the Fusion Neutronics subtask of the IEA Cooperative Program on Nuclear Technology of Fusion Reactors. The work of the Karlsruhe authors was performed within the Nuclear Fusion Programme of this Centre, with support by the European Union.

References

Forschungszentrum Karlsruhe reports (FZKA....) are openly available as .pdf files via http://opac.fzk.de:81/de/fzk_ember_frm.html *(select year, then 1st author and report title, as report numbers are not listed)*

Ci93
S. Cierjacks, P. Obložinsky et al., Fusion Technology 24 (1993) 277-287

Fi02
U. Fischer, S. Simakov et al., to be published at 22nd Symp. on Fusion Technology, Helsinki, September 2002

Ko01
Yu. A. Korovin, A. Yu. Konobeev et al., Proc. Int. Conf. Nuclear Data for Science and Technology (ND2001), October 7-12, 2001, Tsukuba, Japan. Available from the OECD NEA Data Bank, Paris, Program Library Package NEA-156/01, December 2001.

Ma00
F. Maekawa, U. von Möllendorff, M. Wada, P. P. H. Wilson and Y. Ikeda, Fus. Eng. Des. 51-52 (2000) 815-820 (= Proceedings ISFNT-5, Rome, Sept. 1999)

Mö98
U. von Möllendorff, H. Feuerstein and H. Giese, in "Fusion Technology 1998" (B. Beaumont et al., eds.), CEA Cadarache 1998, vol. 2 p. 1445-1448

Mö99
A. Möslang (ed.), IFMIF International Fusion Materials Irradiation Facility Conceptual Design Evaluation Report. Forschungszentrum Karlsruhe report FZKA 6199 (1999), p. 26-28

Mö00
U. von Möllendorff, F. Maekawa, H. Giese and P. P. H. Wilson,
Fus. Eng. Des. 51-52 (2000) 919-924 (= Proceedings ISFNT-5, Rome, Sept. 1999)

Mö02
U. von Möllendorff, H. Tsige-Tamirat, H. Giese and F. Maekawa, Integral activation experiments on fusion relevant materials using a white fast-neutron field. Forschungszentrum Karlsruhe report FZKA 6684 (2002)

Si02
S.P. Simakov, U. Fischer, V. Heinzel and U. von Möllendorff, International Fusion Materials Irradiation Facility (IFMIF): Neutron source term simulation and neutronics analyses of the High Flux Test Module. Forschungszentrum Karlsruhe report FZKA 6743 (2002)

Zi85
J.F. Ziegler, J.P. Biersack and U. Littmark, "The Stopping and Range of Ions in Solids", Pergamon Press (1985)